

000 001 002 003 004 005 006 007 008 009 010 011 012 013 014 015 016 017 018 019 020 021 022 023 024 025 026 027 028 029 030 031 032 033 034 035 036 037 038 039 040 041 042 043 044 045 046 047 048 049 050 051 052 053 EMERGENT BAYESIAN BEHAVIOUR AND OPTIMAL CUE COMBINATION IN LLMS

Anonymous authors

Paper under double-blind review

ABSTRACT

Large language models (LLMs) excel at explicit reasoning, but their implicit computational strategies remain underexplored. Decades of psychophysics research show that humans intuitively process and integrate noisy signals using near-optimal Bayesian strategies in perceptual tasks. We ask whether LLMs exhibit similar behaviour and perform optimal multimodal integration without explicit training or instruction. Adopting the psychophysics paradigm, we infer computational principles of LLMs from systematic behavioural studies. We introduce a behavioural benchmark - BayesBench: four magnitude estimation tasks (length, location, distance, and duration) over text and image, inspired by classic psychophysics, and evaluate a diverse set of nine LLMs alongside human judgments for calibration. Through controlled ablations of noise, context, and instruction prompts, we measure performance, behaviour and efficiency in multimodal cue-combination. Beyond accuracy and efficiency metrics, we introduce a Bayesian Consistency Score that detects Bayes-consistent behavioural shifts even when accuracy saturates. Our results show that while capable models often adapt in Bayes-consistent ways, accuracy does not guarantee robustness. Notably, GPT-5 Mini achieves perfect text accuracy but fails to integrate visual cues efficiently. This reveals a critical dissociation between capability and strategy, suggesting accuracy-centric benchmarks may over-index on performance while missing brittle uncertainty handling. These findings reveal emergent principled handling of uncertainty and highlight the correlation between accuracy and Bayesian tendencies. We release our psychophysics benchmark and consistency metric as evaluation tools and to inform future multimodal architecture designs.

1 INTRODUCTION

The estimation of magnitudes, including quantities like length, duration, or distance, represents one of the most fundamental computations in biological and artificial intelligence. Humans perform these judgments through the Bayesian integration of noisy sensory signals, automatically weighting cues by their reliability (Ernst & Banks, 2002) and incorporating prior expectations to minimise estimation error (Remington et al., 2018; Knill & Pouget, 2004). This computational strategy emerges without explicit instruction across diverse cultures and developmental stages, suggesting it reflects a fundamental solution to information processing under uncertainty.

This universality raises the critical question of whether modern LLMs, trained solely on next-token prediction without explicit perceptual objectives (Radford et al., 2018), spontaneously develop analogous computational strategies. Understanding how LLMs process and integrate uncertain information has immediate implications for building robust multimodal systems that appropriately handle varying input quality (Kendall & Gal, 2017; Ma et al., 2022).

To investigate this, we apply classical psychophysics methodology (Petzschner et al., 2015) to probe these implicit computational strategies in LLMs, treating them as black-box observers and inferring their mechanisms from systematic behavioural analysis. By controlling stimulus uncertainty and measuring characteristic signatures of Bayesian processing, we can determine whether LLMs exhibit human-like optimal perception without explicit training. We found that classic identity mapping tasks, prevalent in psychophysics studies, transfer well to experiments with LLMs and reveal a rich set of patterns. We demonstrate that these controlled tasks serve as necessary 'unit tests'

for multimodal robustness. Unlike naturalistic tasks where noise is unquantifiable, our protocol enables controlled ablations that test for optimal integration strategies, exposing brittleness invisible to standard benchmarks. We present three contributions: 1) We introduce a systematic psychophysics framework for LLMs, a reproducible pipeline for four synthetic magnitude estimation tasks probing length, location, distance, and duration. Our pipeline allows controlled ablations of noise, context, and instruction prompts to track behavioural changes. This framework can serve as infrastructure for future investigations bridging human psychophysics studies 2) We develop a new benchmark: BayesBench based on task performance, cue-combination efficiency, and Bayesian consistency computed with a novel Bayesian Consistency Scores 3) We demonstrate emergent Bayes-consistent behaviour in capable LLMs, while uncovering a critical 'Safety Gap' where highly accurate models fail to adopt robust strategies.

2 RELATED WORK

Human psychophysics. The quantitative study of perception has revealed systematic relationships between physical stimuli and perceptual judgements, formalised in classical laws like Weber-Fechner's logarithmic scaling and Vierordt's temporal regression effects (Fechner, 1860; Weber, 1834; Gibbon, 1977; Jazayeri & Shadlen, 2010; Roseboom et al., 2019; Fountas & Zakharov, 2023). These phenomena, including scalar variability and sequential biases, emerge from optimal Bayesian inference under uncertainty (Petzschner & Glasauer, 2011). When observers estimate magnitudes, they automatically combine noisy measurements with prior expectations, producing characteristic behavioural patterns. Figure 1 illustrates this regression-to-the-mean effect in both Llama-4 Maverick's responses and human psychophysics data—evidence of shared computational principles despite vastly different substrates, as we will see in later sections.

LLMs and Bayesian behaviour. Certain aspects of LLMs are shown to be consistent with Bayesian computation. For example, in-context learning can be interpreted as approximate Bayesian inference (Xie et al., 2021) and, in reasoning, Bayesian teaching is shown to improve performance (Qiu et al., 2025). Similarly, LLMs spontaneously segment sequences using Bayesian surprise in ways that correlate with human event perception (Kumar et al., 2023; Fountas et al., 2025). However, most studies probe explicit reasoning or learned behaviours, where models can leverage acquired statistical rules, rather than perceptual tasks that could reveal computational strategies emerging implicitly from pretraining.

Multimodal studies. Progress have been rapid in developing multimodal LLMs, alongside this is the deployment of benchmarks such as MMbench (Liu et al., 2024) and SEED-bench (Li et al., 2024) that test multimodal reasoning. However, most of these benchmarks do not cover controlled manipulations of modality specific noise for studying fusion strategies. Our synthetic datasets allow fine-grained cue-combination analysis and studies how LLMs combine noisy information from multiple modalities. This is still a nascent area of research but crucial for better understanding how we may build more robust and generalisable models that will behave optimally under uncertainty.

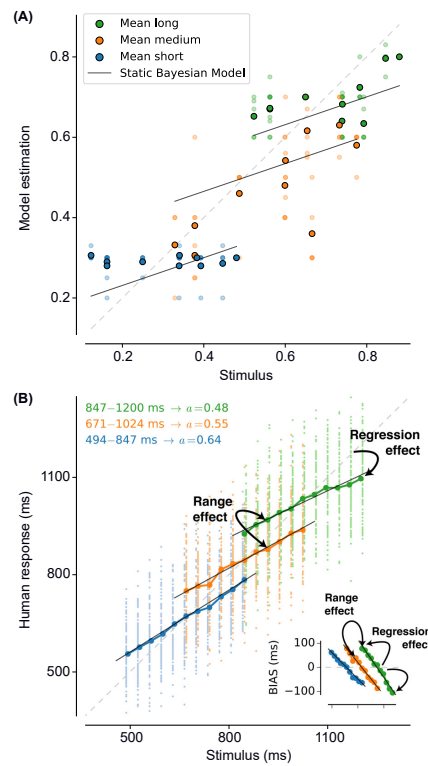


Figure 1: Comparison of LLMs vs human behaviour **A:** Llama-4 Maverick in one of the line length ratio estimation experiments. The fitted lines are based on a static Bayesian observer model. Light dots are individual data points **B:** Response from typical human psychophysics studies (adapted from Thurley, 2016). We see in both that there is a regression to the mean effect, where responses are biased towards the centre of the stimulus range. This is still a nascent area of research but crucial for better understanding how we may build more robust and generalisable models that will behave optimally under uncertainty.

3 METHODS

3.1 ESTIMATION TASKS AND ABLATIONS

We develop four psychophysics-inspired magnitude-estimation tasks illustrated in Figure 2:

- **Marker location estimation:** given a line with a red marker (or '0' in text input) estimate the position of a marker on a line as a number between 0 to 1.
- **Line ratio estimation:** given two lines, estimate the ratio of the shorter line to the longer line.
- **Maze distance estimation:** given a non-self-intersecting path, estimate the straight line distance between start and the end of the path.
- **Duration estimation:** given an extract of a conversation transcript, estimate the duration of the dialogue. Transcripts are extracted from the AMI Meeting Corpus Kraaij et al. (2005).

The first three tasks are multimodal, with text input and image inputs.

We conduct ablations to probe LLMs and analyse changes in behaviours (see Appendix A.3 for ablation details):

- **Steering:** provide additional textual or numerical information in the system prompt. Aimed at studying how LLMs behaviour changes when asked to consider uncertainty in its responses.
- **Noise:** add constant or gradually increasing blur to the image modality. Aimed at studying how LLMs may reweight information in the presence of noise. We chose gaussian noise for its tractability and ubiquity.
- **Context:** change the length of the available history or reversing trial sequence. Aimed at studying how previous context affects behaviour.

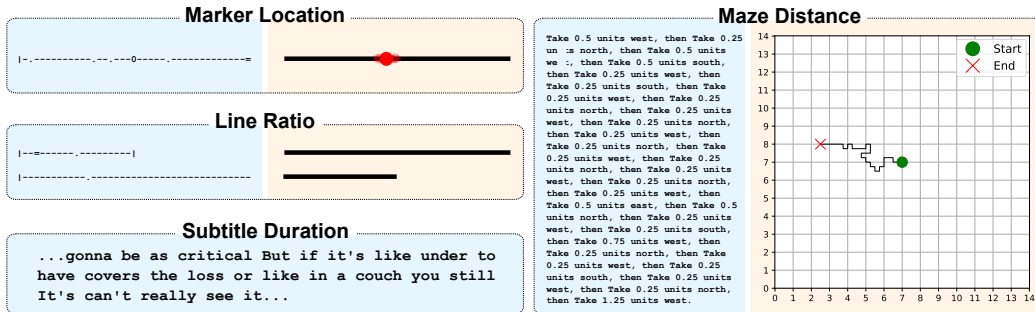


Figure 2: Example of the four magnitude estimation tasks. Cues in a blue background represent information provided as text, while orange represents vision.

3.2 BEHAVIOURAL MODELLING

In human psychophysics studies, participants' responses are fitted against a range of behavioural models to infer their internal computational strategies (Petzschner & Glasauer, 2011; Jazayeri & Shadlen, 2010). This is an effective approach when the subject is essentially a black box, and we can only observe their input-output behaviour. In line with this framework, we fit LLMs' responses against a set of behavioural models covering factors of interest. The degree of fit to different models indicates the extent to which LLMs exhibit that behaviour. Note that while we report model evidence against different behavioural models, we do not rely on individual goodness-of-fit in static conditions to demonstrate Bayesian consistent behavior. Instead, these are used as probes for the Bayesian Consistency Score to study how behaviour changes when experimental conditions are manipulated.

In the below, x_t and y_t denote the true input value of the stimulus and the LLM's estimate at trial t , respectively. μ_t and σ_{dec} are the LLM's internal estimate and response noise level, respectively. We used three main types of behaviour models:

162 **Linear observer.** Linear stimuli-estimation relationship. As our experiments use identity-
 163 mapping tasks, many non-probabilistic heuristics (such as regression to any anchor or fixed biases)
 164 are captured under this relationship

$$165 \quad 166 \quad 167 \quad 168 \quad 169 \quad 170 \quad 171 \quad 172 \quad 173 \quad 174 \quad 175 \quad 176 \quad 177 \quad 178 \quad 179 \quad 180 \quad 181 \quad 182 \quad 183 \quad 184 \quad 185 \quad 186 \quad 187 \quad 188 \quad 189 \quad 190 \quad 191 \quad 192 \quad 193 \quad 194 \quad 195 \quad 196 \quad 197 \quad 198 \quad 199 \quad 200 \quad 201 \quad 202 \quad 203 \quad 204 \quad 205 \quad 206 \quad 207 \quad 208 \quad 209 \quad 210 \quad 211 \quad 212 \quad 213 \quad 214 \quad 215$$

$$\mu_t = wx_t + b, \quad y_t \sim \mathcal{N}(\mu_t, \sigma_{\text{dec}}^2). \quad (1)$$

Static Bayesian observer. LLM’s estimation is a weighted average of the input stimulus x_t and a fixed prior belief μ_p :

$$\mu_t = \frac{\tau_x}{\tau_x + \tau_p} x_t + \frac{\tau_p}{\tau_x + \tau_p} \mu_p, \quad y_t \sim \mathcal{N}(\mu_t, \sigma_{\text{dec}}^2), \quad (2)$$

τ_x and τ_p denote the measurement and prior precisions respectively. We show in the upper panel of Figure 1 an example where this model best fits the LLM’s responses.

Sequential Bayesian observer (Kalman filter). LLM’s estimation is updated trial-by-trial following a standard Kalman filter:

$$\mu_{t|t-1} = \mu_{t-1|t-1}, \quad P_{t|t-1} = P_{t-1|t-1} + q, \quad y_t \sim \mathcal{N}(\mu_t, \sigma_{\text{dec}}^2), \quad (3)$$

Where the update equations are:

$$181 \quad 182 \quad 183 \quad 184 \quad 185 \quad 186 \quad 187 \quad 188 \quad 189 \quad 190 \quad 191 \quad 192 \quad 193 \quad 194 \quad 195 \quad 196 \quad 197 \quad 198 \quad 199 \quad 200 \quad 201 \quad 202 \quad 203 \quad 204 \quad 205 \quad 206 \quad 207 \quad 208 \quad 209 \quad 210 \quad 211 \quad 212 \quad 213 \quad 214 \quad 215$$

$$K_t = \frac{P_{t|t-1}}{P_{t|t-1} + r}, \quad \mu_{t|t} = \mu_{t|t-1} + K_t(x_t - \mu_{t|t-1}), \quad P_{t|t} = (1 - K_t)P_{t|t-1}. \quad (4)$$

r is the measurement noise variance, q is the process noise variance and P is the variance about its estimate. We show in Figure 3 and 4 an example where this model best fits the LLM’s responses. This sequential model is intended to capture within-session inference in a noisy environment. Note that when a model has very high accuracy, response will show little evidence of regression as these are identity mapping tasks. This reinforces the idea that regression effect alone is insufficient and thus the need to introduce alternative probes such as BCS to detect Bayesian behaviours.

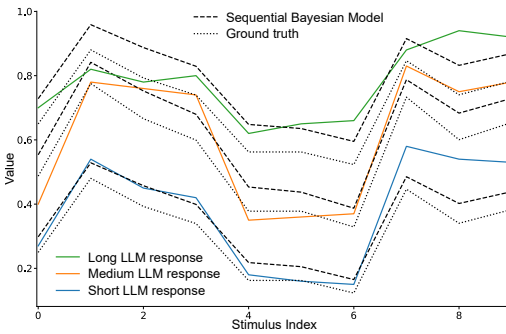


Figure 3: GPT-5 Mini’s mean response (to verbal cues) compared to prediction based on a sequential Bayes model (dotted line)

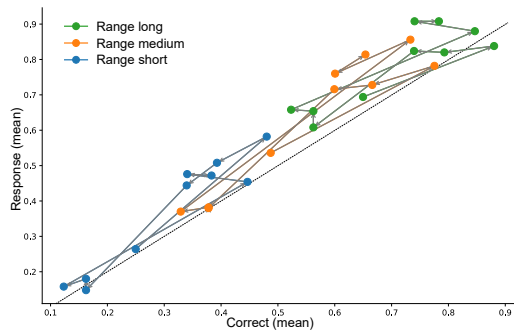


Figure 4: GPT-5 Mini’s mean response trajectory (verbal cue). Arrows denote the sequence of its responses.

Additional model variants Across all models, we include variants with an additional stage of log-transform on the input and output (this mimics studies that support evidence of a logarithmic perception of magnitude in humans and animals (Nieder & Miller, 2003; Nover et al., 2005).)

For non-linear models, we fitted variants where a final stage of gain or affine transformation is applied. This is to account for potential mis-calibration in output mapping (this is not needed for linear models as it is captured in the bias and gradients). Further details can be found in Appendix A.13.

3.3 CUE COMBINATION MODELLING

For our multimodal tasks, we study how LLMs combine text and image cues by modelling their multimodal responses against their unimodal responses. The main models are in Table 1. y_{comb} ,

216	217	218	219	220	221
Equal weighting	Linear regression	Bayes-optimal fusion			
$y_{\text{comb}} = \frac{1}{2}(y_{\text{text}} + y_{\text{image}})$	$y_{\text{comb}} = \alpha y_{\text{text}} + (1 - \alpha) y_{\text{image}}$	$y_{\text{comb}} = w_{\text{text}} y_{\text{text}} + (1 - w_{\text{text}}) y_{\text{image}}$	$w_{\text{text}} = \frac{1/\sigma_{\text{text}}^2}{1/\sigma_{\text{text}}^2 + 1/\sigma_{\text{image}}^2}$		

222 Table 1: Cue-combination baselines. α is fitted in $[0, 1]$. σ_{text}^2 and σ_{image}^2 are the empirical variances
 223 of the LLM’s responses in the text-only and image-only conditions respectively.

224 y_{text} and y_{image} denote the LLM’s response for multimodal, unimodal text and unimodal image,
 225 respectively.

226 For the *Bayes-optimal fusion* model, we report *Oracle* (calibrated, covariance-based) and *Non-
 227 Oracle* (uncalibrated, variance-based) variants. This fusion is the optimal *linear unbiased* combiner
 228 (BLUE) under linear-Gaussian assumptions. See Appendix A.7 for details.

231 3.4 MODEL EVIDENCE

232 Model fit is based on Akaike Information Criterion (AIC). See Appendix A.8 for further details.

235 3.5 KEY METRICS

236 We quantify model along two dimensions: capability as measured by (i) task accuracy and (ii)
 237 cue-combination efficiency, and behaviour strategy as measured by (iii) behavioural consistency.
 238 Separation between capability and behaviour strategy allow us demonstrate cases when they disso-
 239 ciate.

240 **Accuracy (NRMSE).** $\text{NRMSE} = \text{RMSE}_{\text{LLM}} / \text{RMSE}_{\text{baseline}}$, where RMSE has the standard root-
 241 mean-squared-error definition. The baseline is a constant predictor that outputs the mean of the
 242 stimulus range (lower is better).

243 **Efficiency (RRE).** $\text{RRE}(m_{\text{ref}}) = \text{NRMSE}_{\text{ref}} / \text{NRMSE}_{\text{LLM}}$ for any reference combiner m_{ref}
 244 (Sec. 3.3). RRE values > 1 (< 1) mean the LLM has lower (higher) error than the reference.
 245 Note that RRE is used a measure of capability, as it is quantifies the LLM’s performance relative to
 246 a normative baseline, rather as a proof of behaviour or computation strategy.

247 **Bayesian Consistency Score (BCS).** To test whether LLM’s behaviour shifts in the
 248 *Bayes-consistent* direction under controlled ablations, we compare the fitted weights of a static
 249 Bayesian observer model (Sec. 3.2). The posterior mean of this model is precision-weighted with
 250 $w_{\text{prior}} = \tau_p / (\tau_p + \tau_x)$ (prior precision τ_p , measurement precision τ_x), so increasing τ_p or decreasing
 251 τ_x raises w_{prior} . Studying changes in behaviour allow us to compare models which may have very
 252 different static behaviour.

253 We use five ablations across three tasks to compute BCS. These ablations are designed to in-
 254 crease τ_p and/or decrease τ_x : (i) **Steering (verbal)** and (ii) **Steering (unbiased numerical)** provide
 255 range-consistent context or prompt the model about measurement noise, effectively strengthening
 256 the prior ($\tau_p \uparrow$); (iii) **Noise (constant)** and (iv) **Noise (gradual)** blur image inputs to reduce mea-
 257 surement precision ($\tau_x \downarrow$); (v) **Context (longer context window)** supplies a longer rolling history
 258 without altering current measurements ($\tau_p \uparrow, \tau_x$ unchanged).

259 For each ablation a , we compare fitted weights to the base experiment, $\Delta w_{\text{prior}} = w_{\text{prior}}^{(\text{ablation})} - w_{\text{prior}}^{(\text{base})}$,
 260 and set

$$s_a = \begin{cases} +1 & \text{if } \Delta w_{\text{prior}} \geq 0, \\ -1 & \text{if } \Delta w_{\text{prior}} < 0, \end{cases} \quad \text{with } s_a = 0 \text{ if } w_{\text{prior}}^{(\text{ablation})} > 0.9.$$

261 We focus on the *sign* of Δw_{prior} since magnitudes depend on model-specific factors, such how
 262 accurate or noisy a given model’s perception is. For example, a highly perceptually accurate model
 263 may only need to adjust w_{prior} by a smaller amount given an injection of measurement noise. We set
 264 s_a to zero when $w_{\text{prior}}^{(\text{ablation})} > 0.9$, because this indicates a prior-dominant regime, where the model is

Factor	Expression	Parameters
NRMSE (A)	$1 - \frac{\text{NRMSE} - \text{NRMSE}_{\min}}{\text{NRMSE}_{\max} - \text{NRMSE}_{\min}}$	$\text{NRMSE}_{\min, \max} = 0, 2$
RRE (E)	$[\text{RRE}(\text{Bayes Oracle}) + \text{RRE}(\text{Bayes Non Oracle})] / 2$	N/A
BCS (C)	$(\text{BCS} - \text{BCS}_{\min}) / (\text{BCS}_{\max} - \text{BCS}_{\min})$	$\text{BCS}_{\min, \max} = -15, 15$

Table 2: BayesBench components. NRMSE_{\max} is set to 2 (twice the error committed by the constant predictor baseline). $\text{BCS}_{\min, \max}$ are set equal to the range of scores for five ablations across three multimodal experiments.

essentially disregarding the current stimulus and always outputting a constant. This is undesirable because in all five selected ablations the stimulus should remain informative.

The *Bayesian consistency score* sums over ablations: $\text{BCS} = \sum_a s_a$.

3.6 COMPOSITE BENCHMARK SCORE (BAYESBENCH).

The overall *BayesBench score* is a function of three metrics: NRMSE factor for task accuracy (A), RRE factor for cue-combination performance against a Bayes-optimal reference (E) and BCS factor for Bayes-consistency in behaviour adaptation (C) (defined in Table 2). The first factor is averaged across all four tasks while the latter two are averaged across the three multimodal tasks. In the (A) factor, $\text{NRMSE}_{\max} = 2$ defines the upper bound of model NRMSE and models that incur larger error receive no credit. This range spans our model range and marks the worst reasonable performance of any model.

The *BayesBench score* is defined as:

$$S_{\text{BayesBench}} = \frac{1}{3} (A + E + C). \quad (5)$$

BayesBench is designed to provide a holistic summary covering both capability and behaviour across tasks.

4 EXPERIMENTAL SETUP

Each estimation task is divided into three sessions (short, medium, long), where stimulus values fall into different but overlapping ranges per session. The stimuli are generated from a range-uniform prior. This choice enables a clean separation between prior and likelihood and aligns with decades of human psychophysics studies, where range-uniform priors are standard. The overlap in ranges allows us to study context-dependent effects. Figure 5 provides an overview of the stimulus value distributions across sessions, using the marker location as an example. In each session, at each trial, the LLM is given the context of its prior trials (i.e., both the stimulus probes and the LLM’s previous responses, as each API interaction is stateless or “memoryless”). The rolling context simulates how humans form memory of recent interactions, and is the basis of the emergence of Bayesian consistent behaviour. The overall view of our experimental setup is shown in Appendix A.1.

Interactions with LLMs are performed via API. See Appendix A.2 for further details.

We evaluate a diverse set of recent LLMs spanning closed- and open-weight releases (see Appendix A.4 for details). Where possible, we disable extended-thinking or reasoning controls to probe the models’ natural, emergent behaviour. This was feasible for all models except GPT-5 mini, which only allows adjusting reasoning depth; we set this to the lowest level.

In addition, we ran a human baseline study for comparison on all our tasks under a small number of ablations. See Appendix A.5 for details. Human results are included in the left panel of Figure 8. This experiment and analysis are used only as a reference point here, as our main focus is on comparing LLMs against each other. Extensive human psychophysics studies, including the magnitude estimation effects examined here, are extensively documented in psychophysics literature, such as in Jazayeri & Shadlen (2010); Petzschner & Glasauer (2011).

We estimate uncertainty in our results using 30 rounds of bootstrapping while preserving the trial structure within each session to maintain contextual integrity. The error bars shown in Figure 8 and 9 represent 68% bootstrap percentile intervals.

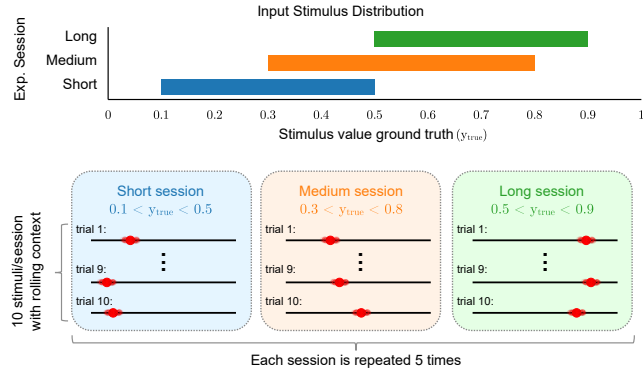


Figure 5: Example distribution of stimulus input for the marker location task

5 RESULTS

5.1 OVERALL PERFORMANCE AND BEHAVIOURAL FIT

Most models perform better in the *text* than the *image* modality, except on the maze distance estimation task. The text input for the maze distance estimation task is a long, detailed path description—much more complex than the ASCII prompts used in other tasks (Fig. 2). Most models perform worse in the text modality for this task, but GPT-5 Mini is an outlier here: it achieves near-perfect text performance, due to the residual reasoning which we can attenuate but not fully disable and shows the task-dependent nature of behaviour. Across tasks, the factor evidence for Bayesian behaviour is consistently higher in the image modality than in text (Appendix A.11).

Moving from unimodal to multimodal inputs does not uniformly improve performance. However, some models are better able to leverage information from the additional modality: Llama-4 Maverick attains its best performance under multimodal conditions across all tasks, and Claude 3.7 Sonnet and GPT-4o improve on two of the three tasks.

Overall, the strongest models (GPT-5 Mini, Claude 3.7 Sonnet, GPT-4o) reach low error rates, comparable to—or better than—human performance (left panel, Fig. 8).

With the exception of Gemini 2.5 Flash Lite, there is a general trend in the left panel of Figure 8 that more accurate models also show stronger evidence of Bayesian behaviour. Note that the relationship between accuracy and behaviour is empirical and is not by necessity. For example, a perfect predictor that maps all stimulus to accurate estimates is indistinguishable from a linear model and can show no probabilistic tendencies.

Under steering ablation, when a numerical range for prior observations is provided in the context prompt, we find that LLMs behavior is strongly affected. As shown in the top right panel of Figure 6, evidence for sequential behavior decreases strongly and in particular, when a deliberately biased numerical range is given, as shown in the left panel of Figure 6, error increases (the triangle icons are generally at larger NRMSE than the circles). This is consistent with the fact that LLMs gravitate their predictions towards prior information provided in-context.

5.2 CUE COMBINATION

From the middle panel of Figure 8, we see that not all models with good NRMSE performance also exhibit efficient cue combination. GPT-5 Mini, despite its strong NRMSE performance, shows poor cue combination efficiency. This is especially pronounced in the maze distance estimation task, where GPT-5 Mini’s performance in the text modality is essentially perfect and much better than

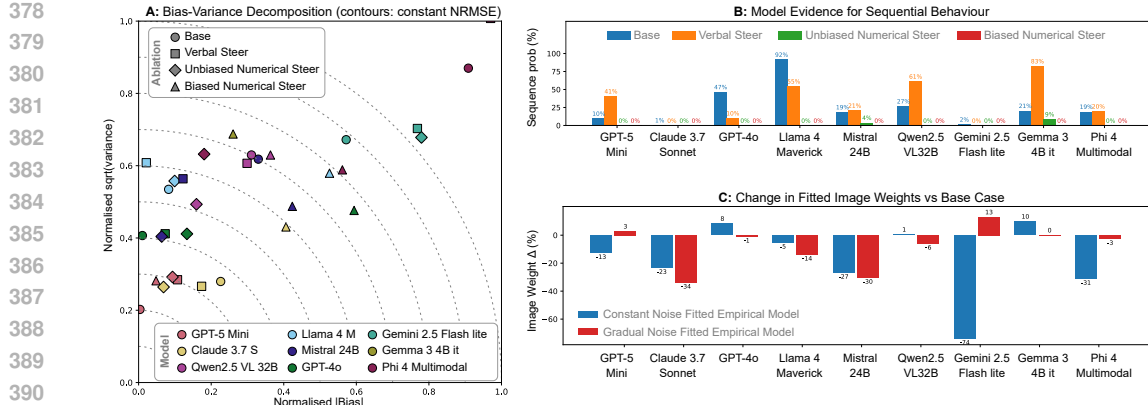


Figure 6: **A:** Bias-variance decomposition under steering ablations. **B:** Impact on sequential model evidence under steering ablation. **C:** Implied image weighting under noise ablation.

its image modality performance. This implies that a Bayes-optimal combination must significantly further downweight its image input. However, it appears unable to downweight its image input to the optimal extent (see Appendix A.12 for further details). On the other hand, in the line length ratio task (see bottom right panel of Figure 6), many LLMs are able to downweight the image modality in the presence of noise, indicating Bayes-consistent adaptation.

Llama-4 Maverick’s multimodal NRMSE performance exceeds that of a Bayesian reliability-weighted unbiased linear combination. The Bayesian reliability-weighted combiner is a normative baseline widely used in biological studies and humans are shown to employ consistent mechanisms Ernst & Banks (2002). Llama-4 Maverick’s outperformance indicates a cue-combination efficiency beyond some biological systems including humans. This suggests that the model may be leveraging additional non-linear properties not assumed under our linear baseline. In Figure 7, we fitted Llama-4 Maverick’s multimodal responses against its unimodal responses. We found that a non-linear random forest is indeed better able to fit its multimodal responses from unimodal responses than linear variants.

Under linear-Gaussian noise, the Bayesian cue combiner is optimal and thus provides a natural yardstick for future improvement on LLMs that have not yet reached this level of performance.

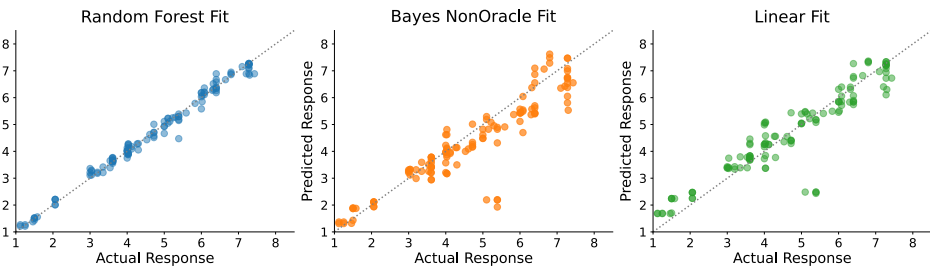


Figure 7: Comparison of cue combination model fits for Llama-4 Maverick. Left panel: random forest fit (blue). Middle panel Bayes-optimal fit (orange). Right panel: linear regression fit (orange).

5.3 BAYESIAN CONSISTENCY

From the right panel of Figure 8, we see that generally more accurate models also tend to exhibit more Bayes-consistent behaviour. However, despite Gemma 3 4B and Phi 4 Multimodal’s lower accuracy, they achieved a decent BCS value. We show a breakdown of the BCS by task and model in A.9.

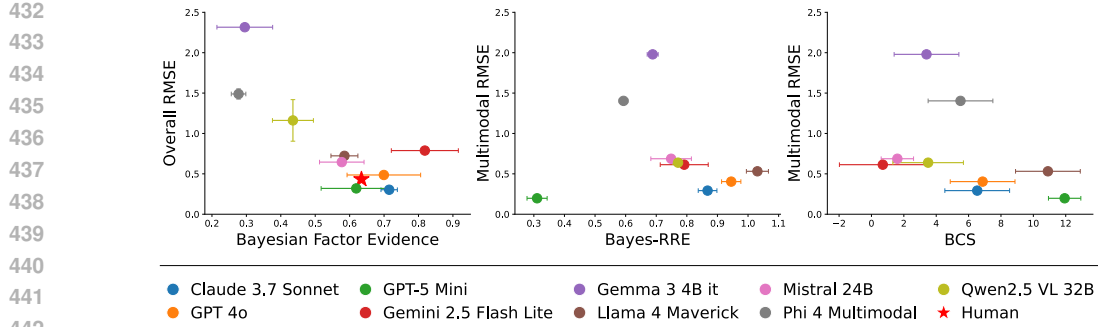


Figure 8: Results summary across models and tasks. Left panel: Bayesian behavioural evidence and relationship against overall NRMSE. Middle panel: cue-combination performance. Shows relationship between multimodal tasks NRMSE and efficiency against Bayes-optimal cue-combination reference models. Right panel: Bayes-consistency score and its relationship against multimodal NRMSE. Each point represents a model, with color indicating model family. Error bars represent 68% bootstrap percentile intervals. Human baseline is shown in the left panel for reference.

5.4 BAYESBENCH SUMMARY

Figure 9 shows the computed BayesBench scores across models, in accordance to the definition in Section 3.6. Bayes-RRE generally increases with accuracy (lower NRMSE), with two notable exceptions: GPT-5 Mini underperforms on Bayes-RRE relative to its NRMSE, whereas Llama-4 Maverick exceeds expectations on Bayes-RRE. BCS likewise tends to track accuracy but provides additional separation among the top models. Overall, Llama-4 Maverick attains the highest BayesBench score, driven by strong Bayes-RRE and BCS components.

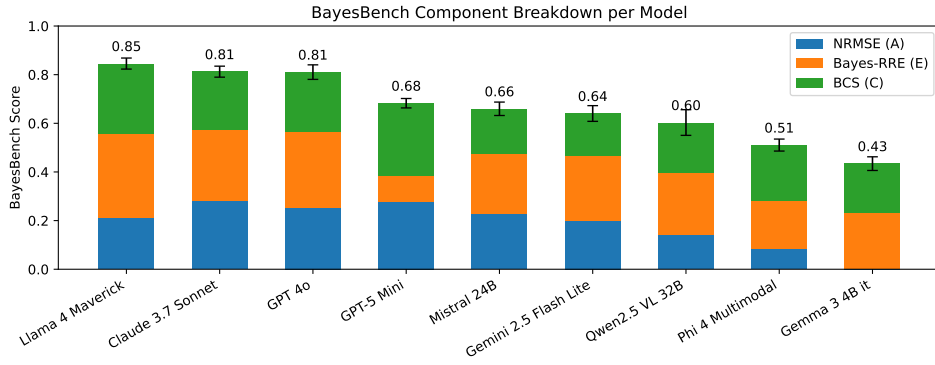


Figure 9: BayesBench overall score, with breakdown into components. Error bars represent 68% bootstrap percentile intervals.

6 DISCUSSION

Our study reveals that LLMs exhibit rich and diverse behavioural patterns when probed with psychophysics-inspired magnitude estimation tasks. While the degree of factor evidence for Bayesian behaviour differs by task and modality, more accurate models (e.g., GPT-5 Mini, Claude 3.7 Sonnet, Llama-4 Maverick) tend to display higher Bayesian factor evidence, especially in the image modality (Appendix A.11 for full breakdown). These models tend to adapt their behaviour in Bayes-consistent ways when inputs are subjected to perturbations such as noise, steering, or extended context (right panel of Figure 8) and take into account contextual prior information during estimation even without explicit training or reasoning instructions. This is reminiscent of findings in human psychophysics, where Bayesian models explain a wide range of human perceptual phenom-

486 ena and processing in the brains (Petzschner et al., 2015; Knill & Pouget, 2004) without explicit
 487 training. We emphasise that our analysis at this stage is behavioural and to offer a mechanistic or
 488 causal account of how such behaviour are implemented would require further analysis.
 489

490 We find that high task accuracy does not always imply optimal cue-combination (middle panel of
 491 Figure 8). For example, GPT-5 Mini attains very low NRMSE yet does not combine modalities
 492 efficiently compared to other models. This shortfall is most apparent when unimodal performance
 493 is imbalanced: optimal behaviour would require the model to markedly down-weight the weaker
 494 modality, which some LLMs fail to do. This has direct practical implications as it exposes the risk
 495 that benchmarks which solely focus on accuracy may favour models with less robustness against
 496 noise. Conversely, Llama-4 Maverick surpasses Bayesian reliability-weighted linear fusion, indi-
 497 cating the use of more sophisticated non-linear integration strategies, consistent with the fact that a
 498 non-linear random forest fits its cue combination better than linear variants.

499 Comparing uni- and multimodal performance reveals that, while models such as Llama-4 Maverick,
 500 Claude 3.7 Sonnet, and GPT-4o are able to utilise the additional modality of input to achieve lower
 501 error when both modalities (text and image) are present for the the majority of multimodal tasks,
 502 this is not a universal trend. The variability in gains indicates potential headroom for advancing
 503 multimodal LLMs. See Appendix A.11 for model-specific breakdown.

504 To capture behavioural features beyond static task metrics, we devised the Bayesian Consistency
 505 Score (BCS) that captures principled behavioural shifts. This allows us to evaluate model behaviour
 506 more holistically, even when accuracy saturates. Measuring behaviour changes under controlled
 507 ablations enable us to compare models that may have different base performance and can offer addi-
 508 tional insights into implicit computational strategies. While more complex heuristics (e.g., salience-
 509 based weighting or rule-switching strategies) may fit static patterns of responses better, it is more
 510 revealing to study Bayes-consistent behaviours under a Bayesian observer model when conditions
 511 change.

512 While LLM behaviours are nuanced and context dependent, our results show that LLMs are gener-
 513 ally consistent with Bayesian observer models. This raises the question of how Bayesian consistent
 514 behaviour can be an emergent property of sufficiently capable models trained on large-scale data,
 515 similar to questions tackled in human studies (Barlow et al., 1961; Wei & Stocker, 2015). Future
 516 architectures or training regimes that better encode uncertainty and support principled cue combi-
 517 nation may improve LLMs’ robustness in noisy, real-world settings. Furthermore, benchmarks such as
 518 our custom BayesBench can complement standard accuracy-based evaluations, offering diagnostic
 519 insights into implicit computational strategies.

520 **Limitations.** As the test range of our tasks is bounded, effects that only emerge with longer se-
 521 quences may not be detected. Our ablation studies are necessarily limited in scope; other perturba-
 522 tions may illustrate different aspects of behaviour. In addition, all interactions relied on API access,
 523 which may be affected by API non-determinism or silent vendor updates.

525 7 CONCLUSION AND FUTURE DIRECTIONS

528 We present BayesBench, a psychophysics-inspired benchmark that probes LLMs’ ability to estimate
 529 magnitudes, integrate noisy multimodal cues, and exhibit Bayes-consistent behaviour. Our findings
 530 show that capable LLMs not only achieve low error rates but also adapt in Bayesian consistent
 531 manners, revealing emergent cognitive-like strategies. Strong multimodal models can also combine
 532 cues efficiently, although this is not guaranteed by high accuracy alone. Our results suggest that
 533 Bayesian-consistent behaviour may emerge naturally in sufficiently capable models.

534 Our work bridges human psychophysics and AI research, by providing both an extensible template
 535 and a set of diagnostic metrics. While our tasks are synthetic, they highlight possible directions
 536 for studying implicit computation in LLMs. The BayesBench framework could be extended to
 537 more naturalistic settings, providing a scaffold for future benchmarks that probe principled cue
 538 combination and uncertainty handling in scenarios closer to real-world use. Future work should
 539 explore representational underpinnings from a mechanistic perspective, and assess how Bayesian
 540 tendencies scale with model size, training data and training objectives.

540 **Reproducibility Statement** We will release *BayesBench* for public use, including the synthetic
 541 data generator, prompts, ablation configurations, behavioural/cue-combination model code and
 542 evaluation scripts. The behavioural models are fully specified in Section 3.2; cue-combination
 543 models are fully specified in Section 3.3; factor-evidence computation in Section 3.4 and Appendix A.8;
 544 the metrics and composite score is specified in Section 3.5 and Appendix A.10;
 545

546 **REFERENCES**
 547

548 Horace B Barlow et al. Possible principles underlying the transformation of sensory messages.
 549 *Sensory communication*, 1(01):217–233, 1961.

550 Marc O Ernst and Martin S Banks. Humans integrate visual and haptic information in a statistically
 551 optimal fashion. *Nature*, 415(6870):429–433, 2002.

553 Gustav Theodor Fechner. *Elemente der Psychophysik*. Breitkopf und Härtel, Leipzig, 1860. English
 554 translation: *Elements of Psychophysics* (Adler, 1966), Holt.

555 Zafeirios Fountas and Alexey Zakharov. Bayesian sense of time in biological and artificial brains.
 556 In *TIME AND SCIENCE: Volume 2: Life Sciences*, pp. 237–265. World Scientific, 2023.

558 Zafeirios Fountas, Martin Benfeghoul, Adnan Oomerjee, Fenia Christopoulou, Gerasimos Lam-
 559 pouras, Haitham Bou Ammar, and Jun Wang. Human-inspired episodic memory for infinite
 560 context LLMs. In *The Thirteenth International Conference on Learning Representations*, 2025.
 561 URL <https://openreview.net/forum?id=BI2int5SAC>.

562 John Gibbon. Scalar expectancy theory and weber’s law in animal timing. *Psychological review*, 84
 563 (3):279, 1977.

565 Mehrdad Jazayeri and Michael N Shadlen. Temporal context calibrates interval timing. *Nature
 566 neuroscience*, 13(8):1020–1026, 2010.

568 Alex Kendall and Yarin Gal. What uncertainties do we need in bayesian deep learning for computer
 569 vision? *Advances in neural information processing systems*, 30, 2017.

570 David C Knill and Alexandre Pouget. The bayesian brain: the role of uncertainty in neural coding
 571 and computation. *TRENDS in Neurosciences*, 27(12):712–719, 2004.

573 Wessel Kraaij, Thomas Hain, Mike Lincoln, and Wilfried Post. The ami meeting corpus. In *Proc.
 574 International Conference on Methods and Techniques in Behavioral Research*, pp. 1–4, 2005.

575 Manoj Kumar, Ariel Goldstein, Sebastian Michelmann, Jeffrey M Zacks, Uri Hasson, and Ken-
 576 neth A Norman. Bayesian surprise predicts human event segmentation in story listening. *Cogni-
 577 tive science*, 47(10):e13343, 2023.

579 Bohao Li, Yuying Ge, Yixiao Ge, Guangzhi Wang, Rui Wang, Ruimao Zhang, and Ying Shan.
 580 Seed-bench: Benchmarking multimodal large language models. In *Proceedings of the IEEE/CVF
 581 Conference on Computer Vision and Pattern Recognition*, pp. 13299–13308, 2024.

582 Yuan Liu, Haodong Duan, Yuanhan Zhang, Bo Li, Songyang Zhang, Wangbo Zhao, Yike Yuan,
 583 Jiaqi Wang, Conghui He, Ziwei Liu, et al. Mmbench: Is your multi-modal model an all-around
 584 player? In *European conference on computer vision*, pp. 216–233. Springer, 2024.

586 Mengmeng Ma, Jian Ren, Long Zhao, Davide Testuggine, and Xi Peng. Are multimodal transfor-
 587 mers robust to missing modality? In *Proceedings of the IEEE/CVF conference on computer vision
 588 and pattern recognition*, pp. 18177–18186, 2022.

589 Andreas Nieder and Earl K Miller. Coding of cognitive magnitude: Compressed scaling of numeri-
 590 cal information in the primate prefrontal cortex. *Neuron*, 37(1):149–157, 2003.

591 Harris Nover, Charles H Anderson, and Gregory C DeAngelis. A logarithmic, scale-invariant rep-
 592 resentation of speed in macaque middle temporal area accounts for speed discrimination per-
 593 formance. *Journal of Neuroscience*, 25(43):10049–10060, 2005.

594 Frederike H Petzschner and Stefan Glasauer. Iterative bayesian estimation as an explanation for
 595 range and regression effects: a study on human path integration. *Journal of Neuroscience*, 31
 596 (47):17220–17229, 2011.

597

598 Frederike H Petzschner, Stefan Glasauer, and Klaas E Stephan. A bayesian perspective on magnitude
 599 estimation. *Trends in cognitive sciences*, 19(5):285–293, 2015.

600 Linlu Qiu, Fei Sha, Kelsey Allen, Yoon Kim, Tal Linzen, and Sjoerd van Steenkiste. Bayesian teach-
 601 ing enables probabilistic reasoning in large language models. *arXiv preprint arXiv:2503.17523*,
 602 2025.

603

604 Alec Radford, Karthik Narasimhan, Tim Salimans, Ilya Sutskever, et al. Improving language under-
 605 standing by generative pre-training. 2018.

606

607 Evan D Remington, Tiffany V Parks, and Mehrdad Jazayeri. Late bayesian inference in mental
 608 transformations. *Nature Communications*, 9(1):4419, 2018.

609

610 Warrick Roseboom, Zafeirios Fountas, Kyriacos Nikiforou, David Bhowmik, Murray Shanahan, and
 611 Anil K Seth. Activity in perceptual classification networks as a basis for human subjective time
 612 perception. *Nature communications*, 10(1):267, 2019.

613

614 Kay Thurley. Magnitude estimation with noisy integrators linked by an adaptive reference. *Frontiers*
 615 in *Integrative Neuroscience*, 10:6, 2016.

616

617 Ernst Heinrich Weber. *De pulsu, resorptione, auditu et tactu: Annotationes anatomicae et physio-*
 618 *logicae*. C. F. Koehler, Leipzig, 1834.

619

620 Xue-Xin Wei and Alan A Stocker. A bayesian observer model constrained by efficient coding can
 621 explain ‘anti-bayesian’ percepts. *Nature neuroscience*, 18(10):1509–1517, 2015.

622

623 Sang Michael Xie, Aditi Raghunathan, Percy Liang, and Tengyu Ma. An explanation of in-context
 624 learning as implicit bayesian inference. *arXiv preprint arXiv:2111.02080*, 2021.

625

626 A APPENDIX

627 A.1 EXPERIMENTAL DESIGN

628 The basic setup of our experiments follows: 1) dataset and prompt generation, 2) session structure
 629 covering the order of stimulus presentation, 3) interation with LLM via API and 4) analyses. This
 630 modular design (Figure 10) allows for systematic exploration of different factors influencing model
 631 performance.

632 A.2 INTERACTION WITH LLMs

633 A.2.1 PROGRAMMATIC API

634 Our interaction with LLMs is through programmatic API calls with temperature fixed at 0.7. As
 635 our aim is to probe the natural, emergent behaviour of highly performant LLMs, we instruct models
 636 not to use reasoning or chain-of-thought, returning only the final numeric answer with minimal
 637 output text. For GPT-5 Mini, reasoning cannot be disabled, so it is set to the lowest reasoning
 638 level available. This provides an additional point of comparison, as reasoning-enabled models may
 639 behave differently in textual tasks. This is something we see in our experiments involving GPT-5
 640 Mini.

641 We emphasise the use of API-based LLMs, some of which are closed source, to ensure our pipeline
 642 is lightweight and easily extended to new models.

643 To test modality dependence, we run tasks in text-only, image-only, and text+image conditions. In
 644 text-only mode, line-ratio and marker-location tasks are represented using ASCII, while the maze
 645 task is described concisely in text. In image-only mode, models receive only the visual stimulus.
 646 In multimodal mode, both text and image inputs are given. This allows us to evaluate efficiency in
 647 unimodal vs multimodal contexts.

648
649
650
651
652
653
654
655
656
657
658
659
660
661
662
663
664
665
666
667
668
669
670
671
672
673
674
675
676
677
678
679
680
681
682
683
684
685
686
687
688
689
690
691
692
693
694
695
696
697
698
699
700
701

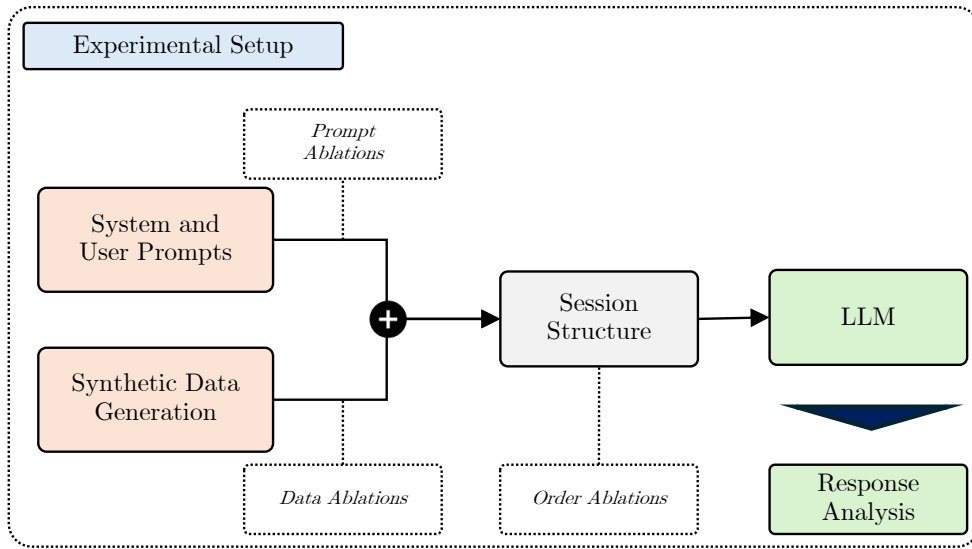


Figure 10: Experimental setup overview

A.2.2 PROMPT DESIGN

For all tasks, prompts are structured in two parts: a **system prompt** and a **user query**.

- **System prompt:** defines the role of the model (e.g., “You are a line-length ratio estimator.”). It specifies the expected output format and instructs the model to *not output reasoning*, but to return only the final numeric estimate (with minimal text if necessary).
- **User query:** provides the stimulus in the chosen modality. In textual mode this is ASCII input (for line ratio and marker tasks) or a concise text description (for maze and subtitle tasks). In image mode only the stimulus image is shown. In multimodal mode both text and image are provided.

Responses that are ill-formed are discarded when we record experimental data.

A typical prompt for the line-length ratio task (textual mode) is:

```

System prompt: "You are a line-length ratio
estimator. Estimate the ratio of the shorter line
to the longer line as a decimal number between 0 and
1. Do not explain or reason. Only output the final
answer."
User input:
| ----- |
```

This design keeps task specification clear and minimises variation in output. For GPT-5 Mini, where reasoning cannot be disabled, we used the lowest reasoning setting. This provides an additional point of comparison, since reasoning-enabled models may behave differently in textual tasks.

For **steering-related ablations**, modifications are made at the system prompt stage. Models may be told that observations are noisy, or given numerical information about the range of past observations. Further details of these manipulations are described in Section A.3.1.

A.3 ABLATION BACKGROUND

Ablation conditions are grouped into three categories: steering-related, noise-related, and context-related. Each modifies the base setup in a controlled way to test specific hypotheses.

702 A.3.1 STEERING-RELATED ABLATIONS
703704 **Verbal cues**

706 • Modified the system prompt to explicitly tell the model that observations are noisy and that
707 it should act in a Bayesian way.
708

709 • Example system prompt:
710 You are a line-length ratio estimator. The given data is noisy and may contain
711 artifacts. You should behave like a Bayesian observer and take into account prior
712 and likelihood in your predictions.

713 **Numerical cues**

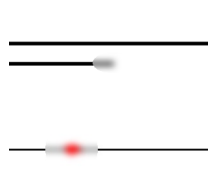
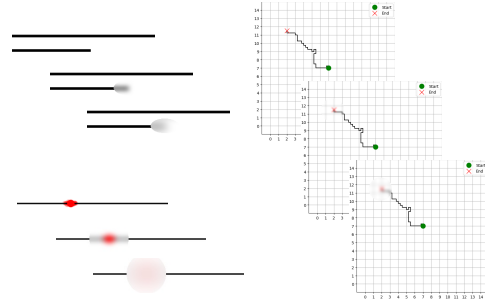
714 • Modified the system prompt to provide the numeric range of the past ten observations,
715 encouraging the model to use this information as a prior.
716

717 • Example system prompt:
718 You are a line-length ratio estimator. The given data is noisy and may contain
719 artifacts. For 10 previous observations, the values were observed to lie in the
720 range of 0.1 to 0.3.

721 A.3.2 NOISE-RELATED ABLATIONS
722

723 **Constant noise:** Applied a Gaussian blur to image inputs only, to test whether models adapt esti-
724 mation behaviour when vision is degraded.

725
726 **Noise sequence:** Introduced gradually increasing Gaussian blur across trials to test whether mod-
727 els downweight visual information as noise grows. Figure 12 shows example input images.

730
731
732
733
734
735
736
737
738
739
740 Figure 11: Constant Gaussian noise ablation

741 Figure 12: Sequential Gaussian noise ablation

742 A.3.3 CONTEXT-RELATED ABLATIONS
743

744 **Shorter Context:** Reduced the context window to 3 prior trials, limiting how much past informa-
745 tion the model can use.

746
747 **Longer context** Increased the context window to 20 prior trials, maximising available history for
748 the model.

749
750 **Stimulus order reversal** Reversed the order of stimuli to test whether model estimations show
751 strong sequence dependence.

752 A.4 LLM MODELS STUDIED
753

754 Table 3 summarises the key characteristics of the LLMs studied. We chose a diverse set of recent
755 models spanning closed- and open-weight releases, with a range of sizes and architectures. Where

756

h

757

758 Table 3: Comparison of selected LLMs (parameters shown only when vendor/model card publicly
759 discloses them).

Model	Developer	Params	Reasoning controls
Claude 3.7 Sonnet	Anthropic	Undisclosed	Optional “extended thinking”
GPT-5 Mini	OpenAI	Undisclosed	Adjustable depth.
GPT-4o	OpenAI	Undisclosed	N.A.
Llama-4 Maverick	Meta	400B total / 17B active	N.A.
Qwen 2.5 VL 32B	Alibaba	32B	N.A.
Mistral 24B	Mistral	24B	N.A.
Gemini 2.5 Flash Lite	Google DeepMind	Undisclosed	N.A.
Phi 4 Multimodal	Microsoft	Undisclosed	N.A.
Gemma 3 4B	Google DeepMind	4B	N.A.

760
761 **Notes:** We avoid speculative parameter estimates. Public sources: Claude 3.7 Sonnet announcement
762 (Anthropic); GPT-5 Mini (OpenAI docs); Llama-4 Maverick active/total params (Meta); Qwen 2.5-VL 32B
763 model card; Mistral 24B (Mistral docs); Gemini 2.5 Flash-Lite (Google); Phi-4 Multimodal (Microsoft HF
764 card); Gemma 3 model card.

765 possible, we disabled extended-thinking or reasoning controls to probe the models’ natural, emer-
766 gent behaviour. This was feasible for all models except GPT-5 Mini, which only allows adjusting
767 reasoning depth; we set this to the lowest level.

768 A.5 HUMAN FEEDBACK COLLECTION

769 We collected data from human subjects on our main tasks to establish a calibration benchmark. The
770 questions are hosted on a web platform, and users can complete them with their phone or computer.
771 Only two ablations were used for human feedback collection: constant noise and longer context.

772 Figure 13 shows two screenshots of the web platform.

773 A.6 ETHICS STATEMENT

774 Our human baseline study involved a minimal-risk web-based questionnaire where participants pro-
775 vided perceptual judgments on magnitude estimation tasks. Participation was voluntary, partici-
776 pants provided informed consent via the web platform, could withdraw at any time, and all data was
777 anonymized. No personal, sensitive, or identifiable information was collected.

778 A.7 BAYES CUE COMBINATION MODELS

779 Under Bayesian assumptions, the optimal linear combination of two noisy modality estimates is
780 obtained by weighting them according to their relative reliabilities (inverse variances. See also Ernst
781 & Banks (2002)). We consider two versions. Non-oracle and oracle models. They differ in whether
782 the cue combination is modelled with or without access to ground truth.

783
784 • **Non-oracle:** The model combines the two modality estimates ($\mu^{(1)}$ and $\mu^{(2)}$) by inverse-
785 variance weighting,

$$786 \mu = \frac{\tau_1}{\tau_1 + \tau_2} \mu^{(1)} + \frac{\tau_2}{\tau_1 + \tau_2} \mu^{(2)},$$

787 where $\tau_i = 1/\sigma_i^2$ are the precisions of estimates from the corresponding modality. Cru-
788 cially, the model does not assume access to ground truth. It only uses the variance of each
789 modality estimate to compute the above weighting.

790
791 • **Oracle:** In this case, we first calibrate the modality-specific estimates ($\mu^{(1)}$ and $\mu^{(2)}$) by
792 fitting gain and offset parameters to the ground truth for each modality. After calibration,
793 the estimates ($\mu'^{(1)}$ and $\mu'^{(2)}$) are combined using the generalised least squares solution

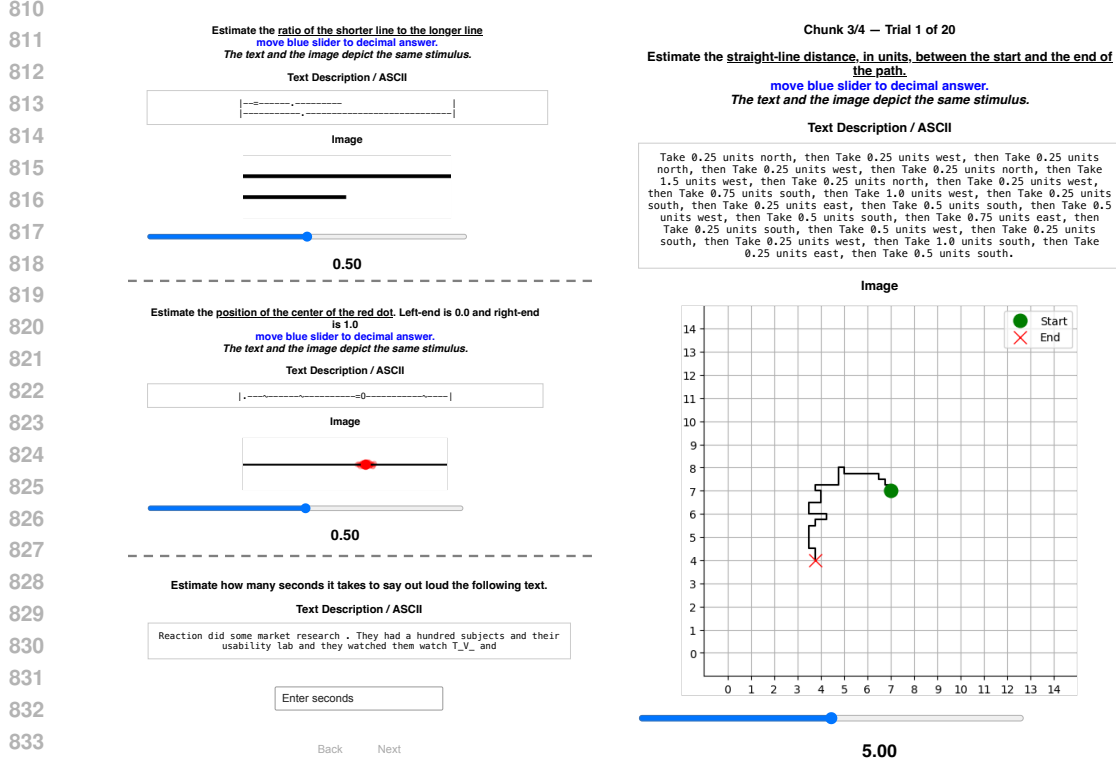


Figure 13: Human feedback collection website screenshot

based on the residual loss covariance (Σ):

$$\mu = \frac{\mathbf{1}^\top \Sigma^{-1} \mu'}{\mathbf{1}^\top \Sigma^{-1} \mathbf{1}},$$

where $\mu' = \begin{bmatrix} \mu'^{(1)} \\ \mu'^{(2)} \end{bmatrix}$ and Σ is the 2×2 covariance matrix of the modality estimates. This accounts for both differing reliabilities and cross-modal correlations, yielding the optimal linear unbiased estimator given access to the true values.

Although these models specify optimal *linear* integration strategies, it is important to note that LLMs may, in principle, outperform these baselines if they achieve more flexible, nonlinear forms of cue integration. Such nonlinear integration is possible given the architecture of modern LLMs.

A.8 FACTOR ANALYSIS DETAILS

We fit many behavioural model variants that differ along interpretable *factors* (e.g., BAYESIAN vs NON-BAYESIAN; WEBER vs NON-WEBER; SEQUENTIAL update). Because these variants partly overlap in purpose, naively summing or averaging likelihoods would (i) reward families that contain more variants, or (ii) dilute good variants by pooling with weak ones. We therefore compare *factors* while treating all other dimensions as *nuisance*.

Procedure Let $f \in \{\text{BAYESIAN}, \text{WEBER}, \text{SEQUENTIAL}\}$ be the factor of interest, and let $\mathcal{N}(f)$ denote the set of nuisance factors for this comparison (chosen to be agnostic to f ; see example below).

1. **Transform AIC to likelihood.** For each fitted variant m , first compute $\Delta \text{AIC}(m)$ (defined as the difference between m 's AIC and the minimum AIC among all variants) and then

864 compute the transformed quantity below:
 865
 866
$$L(m) \propto \exp\left(-\frac{1}{2} \Delta \text{AIC}(m)\right),$$

867 2. **Group by nuisance “cells”.** Group behavioural models by every combination of values in
 868 $\mathcal{N}(f)$. Each group is a cell c .
 869 3. **Best-in-cell for each level of f .** Within each cell c , take the *maximum* likelihood among
 870 variants where $f = \text{True}$ and among variants where $f = \text{False}$:

872
$$L_{\text{True}}^{(c)} = \max_{m \in c, f(m)=\text{True}} L(m), \quad L_{\text{False}}^{(c)} = \max_{m \in c, f(m)=\text{False}} L(m).$$

 873

874 Using the max avoids penalising a family for having many weak sub-variants.

875 4. **Equal-weight across cells.** For fairness, average *equally* across cells where both levels are
 876 present (intersection):

877
$$\bar{L}_{\text{True}} = \frac{1}{|C|} \sum_{c \in C} L_{\text{True}}^{(c)}, \quad \bar{L}_{\text{False}} = \frac{1}{|C|} \sum_{c \in C} L_{\text{False}}^{(c)},$$

 878

880 where $C = \{c : L_{\text{True}}^{(c)}, L_{\text{False}}^{(c)} \text{ both defined above in step 3.}\}$.
 881

882 5. **Compute evidence.** Report the factor-level probability

883
$$P(f=\text{True} \mid \text{data}) = \frac{\bar{L}_{\text{True}}}{\bar{L}_{\text{True}} + \bar{L}_{\text{False}}},$$

 884

885 and similarly for False .
 886

887 In this report when we refer to *factor evidence*, we are always referring to evidence computed from
 888 this procedure.
 889

890 **Example: BAYESIAN vs NON-BAYESIAN.** For $f = \text{BAYESIAN}$ we take $\mathcal{N}(f) = \{\text{WEBER}\}$
 891 only. The SEQUENTIAL and GAIN variants exist exclusively within the Bayesian family; conditioning
 892 on them would create empty cells on the non-Bayesian side. Thus, within each WEBER cell
 893 we compare the best Bayesian variant (possibly sequential/gain/log) against the best non-Bayesian
 894 variant, average equally over cells, and form the head-to-head probability. Below table shows the
 895 procedure schematically.

896

	WEBER cell	
	False	True
Best Bayesian in cell	$L_{\text{True}}^{(c)}$	$L_{\text{True}}^{(c)}$
Best non-Bayesian in cell	$L_{\text{False}}^{(c)}$	$L_{\text{False}}^{(c)}$

900 *Average equally across cells, then compute $P = \bar{L}_{\text{True}} / (\bar{L}_{\text{True}} + \bar{L}_{\text{False}})$.*
 901

902 **Notes on fairness and robustness.** (i) Equal cell weighting prevents families with many variants
 903 from accruing more probability mass simply by proliferation. (ii) Using the intersection of cells
 904 avoids bias from missing combinations.
 905

906 A.9 BCS BREAKDOWN BY EXPERIMENT

907 We show below the breakdown of BCS score by experiment and task.
 908

909 A.10 BCS FITTING DETAILS

910 We fit the static Bayesian observer model in all cases and with data from modalities according to the
 911 below:
 912

913

- 914 • **Noise:** evaluate w_{prior} from the *image-only* modality, since noise is injected only into the
 915 image channel and multimodal fits would confound reweighting of text input.
- 916 • **Steering and Context:** evaluate w_{prior} from the *multimodal* fit, as these manipulations
 917 affect both modalities.

Model	Line Ratio	Marker Location	Maze Distance
Claude 3.7 Sonnet	1.5	5.0	0.0
GPT 4o	0.8	4.5	1.5
GPT-5 Mini	5.0	5.0	1.9
Gemini 2.5 Flash Lite	1.7	-1.3	0.3
Gemma 3 4B it	1.1	0.8	1.5
Llama 4 Maverick	3.2	4.4	3.3
Mistral 24B	1.5	1.0	-0.9
Phi 4 Multimodal	2.4	1.3	1.8
Qwen2.5 VL 32B	-2.0	5.0	0.5

Table 4: Model-wise BCS score across experiments

A.11 MODEL PERFORMANCE AND BAYESIAN FACTOR EVIDENCE

Figures 14, 15, 16 and 17 show the NRMSE performance and Bayesian factor evidence for all models across all tasks and modalities. For the multimodal tasks, in their corresponding figures, metrics by modality is shown over the three rows.

Notice that not all models perform better in multimodal conditions than in unimodal conditions (Llama-4 Maverick is the outlier, it achieves its best NRMSE in multimodal mode on all tasks).

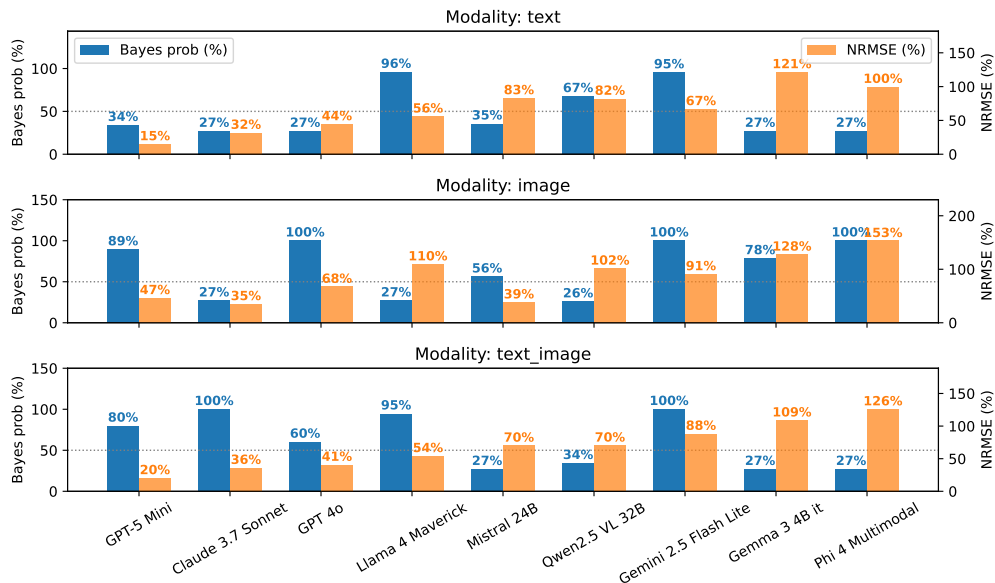


Figure 14: Line length ratio estimation task. NRMSE and Bayes factor evidence for unimodal text, unimodal image and multimodal inputs.

A.12 GPT-5 MINI CUE COMBINATION MODEL FITS

GPT-5 Mini’s cue-combination performance is poor despite its very strong NRMSE performance. Figure 16 shows the NRMSE performance for each model in all three modalities for the maze distance estimation task. We see that GPT-5 Mini’s unimodal text performance is nearly perfect (at 0.01 NRMSE), while its unimodal image performance is much worse (at 0.2 NRMSE, despite already being the best across models). Because of this, the Bayes-optimal linear combination would imply a nearly zero weighing on the image input. However, the multimodal performance does not follow this trend, indicating that the model prediction is still affected by the image input.

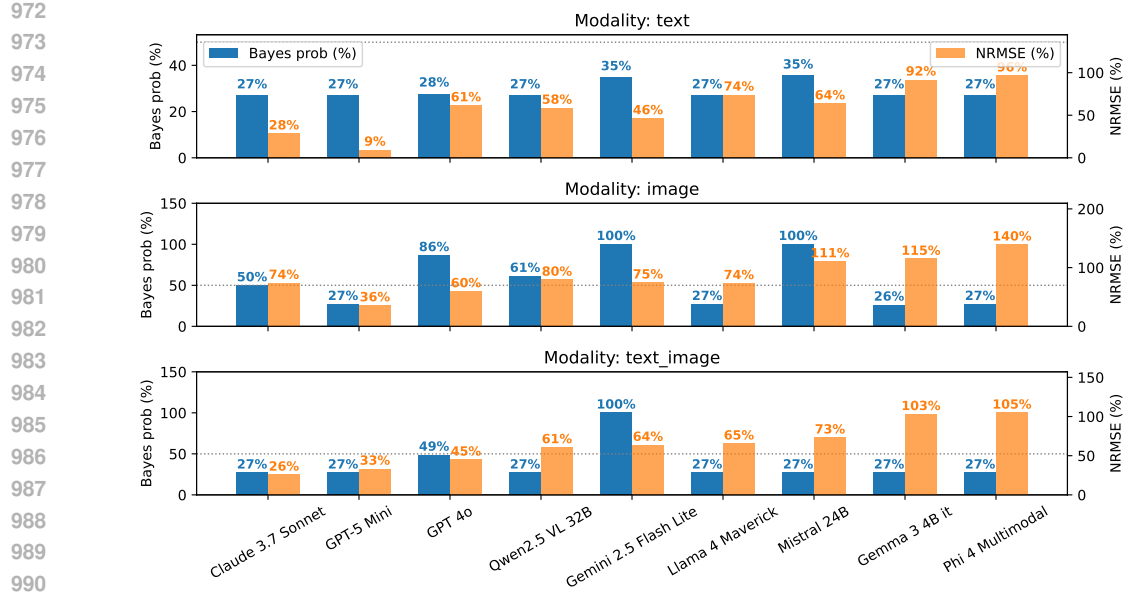


Figure 15: Marker location estimation task. NRMSE and Bayes factor evidence for unimodal text, unimodal image and multimodal inputs.

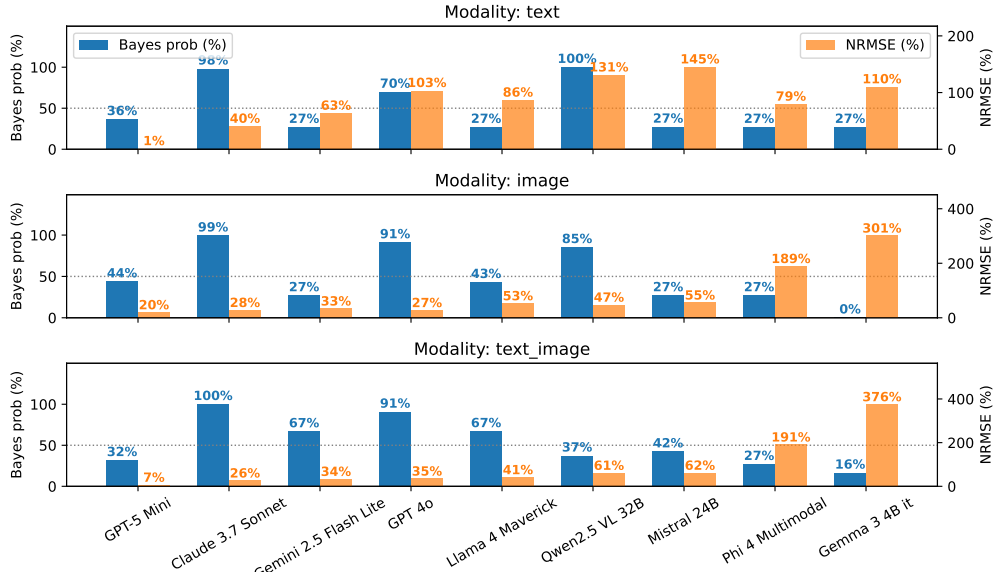


Figure 16: Maze distance estimation task. NRMSE and Bayes factor evidence for unimodal text, unimodal image and multimodal inputs.

A.13 FURTHER MODEL VARIANTS

Studies such as (Nieder & Miller, 2003; Nover et al., 2005) found in human studies that the human brain encodes many different magnitudes using a logarithmic scale. To test if this phenomena apply in LLM, we explored variants of models where a logarithmic transform is applied to the stimulus values.

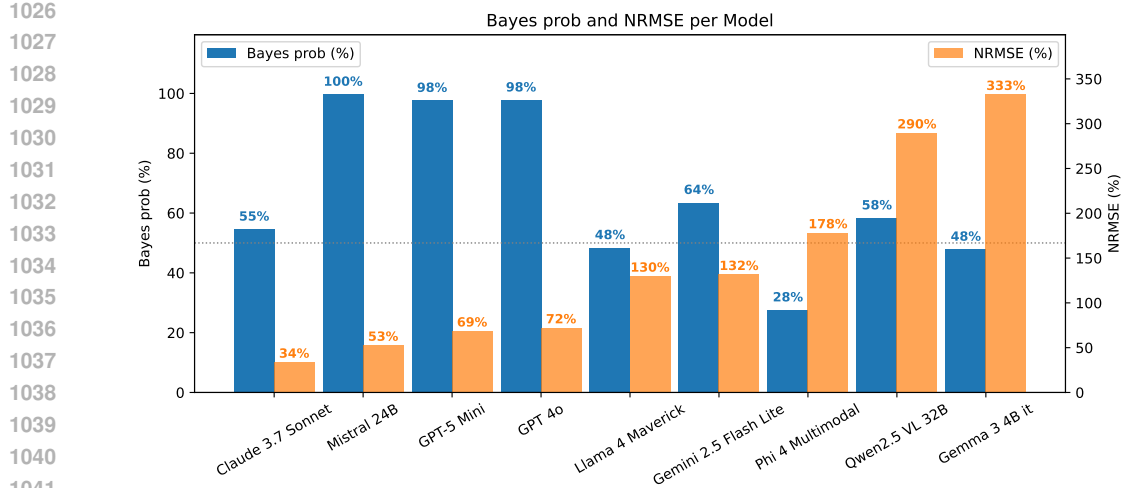


Figure 17: Subtitle duration estimation task. NRMSE and Bayes factor evidence.

For the Bayesian model we also added variants with an affine transform after the estimate is computed, to account for any potential gain biases. This is not needed for the linear models as it is captured by the gradient parameter.

Note that for all these variants, the additional parameters will penalise AIC and therefore help guard against artificial model evidence inflation by more complex models.

A.13.1 LOGARITHMIC TRANSFORM

In some model variants, a logarithmic transform is applied to the stimulus or response space before fitting our behavioural models above. This is motivated by standard assumptions in psychophysics that humans internally represent magnitudes on a log scale.

Thus the transformed stimulus x'_t from the raw input x_t is

$$x'_t = \log(x_t + \epsilon),$$

with a small ϵ ensuring numerical stability. Log-transform variants are considered for both the linear and Bayesian observer models.

A.13.2 AFFINE TRANSFORM

For Bayesian models, we additionally allow affine deviations of the posterior estimate, corresponding to a gain factor $g \in \mathbb{R}^+$ and an additive offset $\delta \in \mathbb{R}$. The raw posterior mean μ_t from the model estimate is transformed to $\tilde{\mu}_t$ as

$$\tilde{\mu}_t = g \mu_t + \delta.$$

The LLM response y_t in these variants is generated as below, where σ_{dec}^2 is again a free parameter fitted during the model fitting stage:

$$y_t \sim \mathcal{N}(\tilde{\mu}_t, \sigma_{\text{dec}}^2).$$

This captures systematic deviations from the normative Bayesian solution, such as under- or over-weighting of evidence and constant response bias. Note that for linear models this is not required as it is already captured by the slope and offset parameters.